

Non-Uniformity Correction of Infrared Images Based on Improved CNN With Long-Short Connections

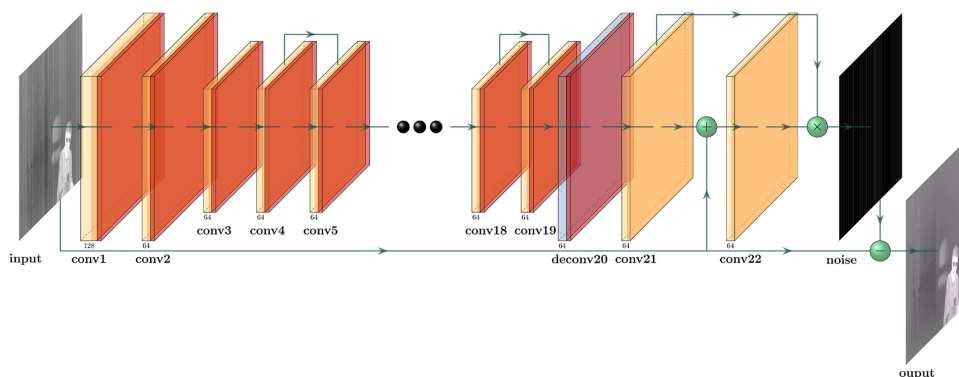
Volume 13, Number 3, June 2021

Timing Li

Yiqiang Zhao, *Member, IEEE*



Yao Li

Guoqing Zhou, *Senior Member, IEEE*



DOI: 10.1109/JPHOT.2021.3080834

Non-Uniformity Correction of Infrared Images Based on Improved CNN With Long-Short Connections

Timing Li ^{1,2}, Yiqiang Zhao,^{1,2} *Member, IEEE*, Yao Li ^{1,2}
and Guoqing Zhou,¹ *Senior Member, IEEE*

¹School of Microelectronics, Tianjin University, Tianjin 300072, China

²Tianjin Key Laboratory of Imaging and Sensing Microelectronic Technology, Tianjin University, Tianjin 300072, China

DOI:10.1109/JPHOT.2021.3080834

This work is licensed under a Creative Commons Attribution 4.0 License. For more information, see <https://creativecommons.org/licenses/by/4.0/>

Manuscript received April 16, 2021; accepted May 13, 2021. Date of publication May 17, 2021; date of current version May 31, 2021. This work was supported by National Key R&D Program of China under Grant 2018YFB1304700. Corresponding author: Timing Li (e-mail: litm@tju.edu.cn).

Abstract: Non-uniformity is a common phenomenon in infrared imaging system, which seriously affects imaging quality. In view of the problems of existing non-uniformity correction of infrared images, such as loss of image details and blurred edge of image, an improved non-uniformity correction method of infrared images based on convolution neural network using long-short connections (LSC-CNN) is proposed. The proposed method designs a long-short connection residual network structure suitable for non-uniformity correction of infrared image. The network depth is increased to fully learn the noise by short connections, image sizes are adjusted to reduce the number of parameters, the long connection is used to solve the problem of image information loss caused by transposed convolution, and a multiply operation is carried out to enhance the contrast of corrected images. Besides, batch normalization is utilized to improve the training speed. The experimental results show that LSC-CNN has excellent performance in non-uniformity correction of infrared images whether qualitative evaluation or quantitative evaluation. LSC-CNN is especially effective in image detail preservation and image edge protection whose average PSNR exceeds 37.5 dB and the average SSIM is greater than 0.98.

Index Terms: Infrared image, non-uniformity correction, combination of long and short connections, improved neural network.

1. Introduction

The non-uniformity in the infrared imaging systems seriously affects the imaging quality, which is mainly manifested as fixed-pattern noise (FPN). The main reasons are as follows: firstly, because the manufacturing process is not mature, response of the infrared focal plan array (IRFPA) unit is inconsistent; secondly, in order to reduce the manufacturing cost of IRFPA, the same amplifier is shared among the detector units in the same column or row, and the magnification cannot be completely consistent; thirdly, compared with the cooled infrared detector, the operating temperature and the ambient temperature of the electronic devices in the uncooled infrared detector also affect the response characteristics of each detection unit [1], [2]. Therefore, the non-uniformity correction of infrared image is not only the key to improve the quality of infrared image, but also the research focus of infrared image processing. The response of each detector in IRFPA can be approximated

by a liner model [3], [4], as shown in (1).

$$y_{ij} = g_{ij} * x_{ij} + o_{ij} \quad (1)$$

where y_{ij} is the response of the (i, j) detector, x_{ij} is the real infrared radiation received by the (i, j) detector, g_{ij} and o_{ij} denote the gain noise and offset noise, respectively.

Compared with visible images, infrared images have lower contrast, so it is necessary to enhance infrared images [5]–[7]. Meanwhile, infrared images have less detail information than visible images, so the image quality will be seriously affected if the noise removals are not enough. To resolve these issues, this paper applies deep-learning to non-uniformity correction of infrared image, establishes a noise simulation model, learns the noise characteristics of infrared images, and separates the noise in the input noisy image. The convolution layer and deconvolution layer with strides size of 2 reduce the calculated cost. Compared with the existing non-uniformity correction methods, the proposed method achieves excellent performance and is especially effective in image detail preservation and image edge protection.

To summarize, the main ideas and contributions of this paper are as follows:

- 1) Different from the existing scene-based non-uniformity correction algorithms, the long-short connections can effectively alleviate the problem of gradient vanishing/explosion, and solve the problem that the existing methods based on neural networks cannot adequately remove FPN from infrared image and cannot accurately retain image details because of the insufficient network depth.
- 2) A multiply operation is carried out with the data before and after long connection, which can effectively solve the problem of reduced contrast after infrared image non-uniformity correction, and simultaneously preserve the edge information better in the infrared image.
- 3) The image size adjustment effectively reduces the number of parameters of LSC-CNN and reduces the model computation time. Meanwhile, the batch normalization is introduced to improve the training speed and training stability of the model.

The remainder of the paper is organized as follow. Section 2 provides a brief survey of related work. Section 3 introduces the LSC-CNN method in detail. Section 4 compares and evaluates the performance of the LSC-CNN method. Finally, it is summarized in Section 5.

2. Related Work

At present, the most representative methods in the field of image denoising, such as GF [8], BM3D [9] and DnCNN [10]. However, because of infrared images have the characteristics of low resolution, low contrast and low signal-to-noise ratio, these methods are not ideal for infrared image denoising. They are easy to blur the image and lose image information. Therefore, the application of visible light image correction methods in the field of infrared image non-uniformity correction is limited.

In order to correct the non-uniformity of IRFPA, the existing non-uniformity correction methods can be divided into two categories: calibration-based nonuniformity correction (CBNUC) and scene-based non-uniformity correction (SBNUC).

CBNUC determines the gain and bias by using uniform temperature blackbody or shutter as a reference, such as two-point method [11], [12] and multipoint method [13], [14]. CBNUC is widely used in infrared imaging system because of simple implementation and low computational complexity. However, after an infrared detector works for a period of time, the working temperature of the detector changes and the response characteristics drift, which makes the initial correction parameters of CBNUC invalid. Therefore, the infrared imaging system needs periodic shutdown to obtain new correction parameters for reference sources, which limits the use of CBNUC in the field of infrared video security monitoring and early warning [15], [16].

To solve the problem that CBNUC cannot work continuously for a long time, SBNUC was proposed, such as Kalman-filtering [17], constant-statistics constraint [18], [19], temporal high pass filter [20] and neural network [21], [22]. SBNUC can effectively solve the problem that the CBNUC

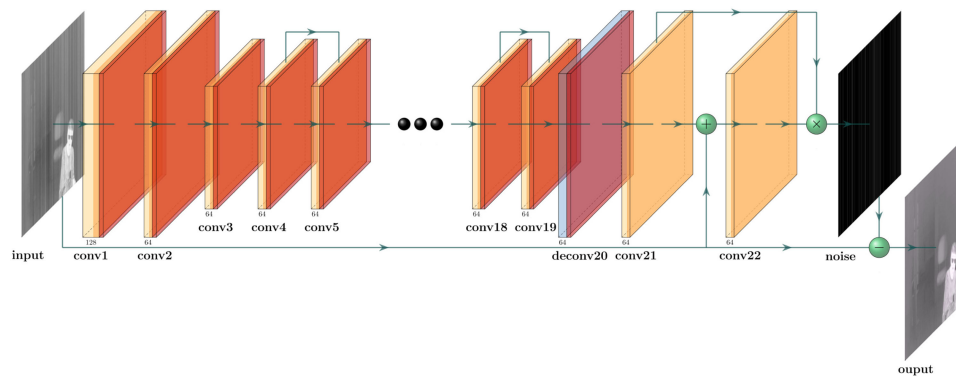


Fig. 1. Architecture of LSC-CNN predictive model.

cannot work continuously, so the research in recent years is mainly focused on SBNUC. The non-uniformity correction method based on neural network has good adaptability and anti-noise ability, but the traditional neural network algorithm will lead to blurring edges and artifact phenomenon.

To overcome the disadvantages of neural network algorithm, researchers have improved the neural network non-uniformity correction algorithm. At present, Lai *et al.* [23] proposed the bilateral total variation algorithm, which reduces the nonuniformity and suppresses artifacts phenomenon by introducing regularization, however, there are still residual FPN and artifacts in the images. Kuang *et al.* [24] proposed SNRCNN, which adopts a deep convolution neural network and can process images quickly, but there is a phenomenon of underfitting. Li *et al.* [25] improved a learning rate rule that combines adaptive threshold edge detection and time gate, which divides the non-uniformity correction process into two parts: denoising and artifact removal, although this algorithm achieves good results, the added edge detection and adaptive threshold calculation will increase computational burden. Li *et al.* [26] preprocessed the input layer by adding a learning layer to protect the image information and eliminate the low-frequency noise, although this method can improve the image quality, it will reduce the image contrast.

In recent years, with the continuous increase of image data and the continuous improvement of hardware performance, more and more artificial intelligence methods have been introduced, in which deep learning has a better performance in the field of image processing. He *et al.* [27] proposed the deeplearning-based strip non-uniformity correction method (DLS-NUC), which adopts the residual network architecture with large receptive field to obtain better processing results, however, it will reduce the contrast. Guan *et al.* [28] adopted a wavelet deep neural network to remove the FPN of the image by using the special characteristics of stripe noise and complementary information between the coefficients of different wavelet sub-bands, whereas this method has some disadvantages such as large computation and detail loss under strong noise level.

3. Methodology

Different from existing neural network algorithms that learn the mapping relationship between noisy-free and noisy infrared images, the proposed LSC-CNN reconstructs the residual information and uses original images to offset the reconstructed noisy images to obtain the corrected images. The LSC-CNN predictive model architecture is shown in Fig. 1. The uncorrected infrared images are input into the network model and processed to obtain the corrected uniform infrared images.

The LSC-CNN includes features extraction, size adjustment, residual block and image restoration. The first layer uses a larger convolution kernel to extract features from the image, as shown in (2).

$$M = W * I + B \quad (2)$$

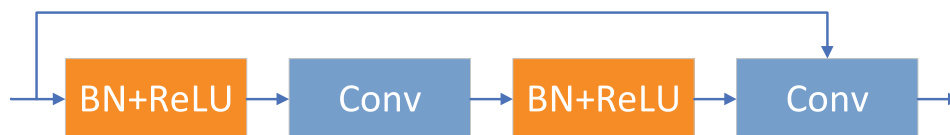


Fig. 2. Architecture of a short connection.

TABLE 1
Configurations of Model Parameters

Layers	Filter size	Filter number	stride
Input	-	-	-
Conv1	3*3	128	1
Conv2	3*3	64	1
Conv3	3*3	64	2
Residual block	$\begin{bmatrix} 3 \times 3 \\ 3 \times 3 \end{bmatrix} * 8$	$\begin{bmatrix} 64 \\ 64 \end{bmatrix} * 8$	$\begin{bmatrix} 1 \\ 1 \end{bmatrix} * 8$
Deconv	3*3	64	2
Conv21	3*3	1	1
Concate	Input + Conv21		
Conv22	3*3	1	1
Multiply	Input \circ Conv21		
Output	-	-	-

where M is the feature maps, W and B are weights and biases respectively, $*$ represents convolution operation, and I is the input noisy image. In order to reduce the number of model parameters, the second layer uses a smaller convolution kernel to extract features again and reduce filters. The third convolutional layer reduces the image size by using a large step size to achieve a reduced computational effort. For the sake of solving the problem of vanishing/exploding gradients with the increase of network layers, a short connection is adopted to connect every two convolution layers together, the structure is shown in Fig. 2. The short connections can effectively alleviate the problem of vanishing gradients and maintain good performance in deeper neural network models.

The deconvolution layer is set up to restore the image to its original size. A grayscale image is generated from the transposed convolved image by using a convolution layer with a filter size of 1. A long connection between the transposed convolution layer and the input layer is used to compensate for the information loss caused by transposed convolution, and a two-dimensional grayscale image is generated by the convolution layer with a filter size of 1. The two images before and after compensation are multiplied by pixels, which strengthens the contrast of the image and generates the reconstructed noise map. Ultimately, the noise-containing image P output by the FPN module is offset with the noisy image N generated by the neural network to generate the denoised image $F_{denoise}$, as shown in (3).

$$F_{denoise} = P - N \quad (3)$$

4. Experimental Results

4.1 Implementation Details

The LSC-CNN has a total of 22 layers. The parameters of each layer are shown in Table 1. The first layer extracts feature by using 7*7 large kernel with the step size of 1, and establishes 128 filters.

TABLE 2
Comparison of Average Results for 269 Frames With or Without Long and Short Connections and With or Without Size Adjustment Results

Models	AVG PSNR	AVG SSIM	AVG Time
With short connections and size adjustment	37.5128	0.9808	0.0445
With short connections but without size adjustment	36.5219	0.9778	0.0727
Without short connection but with size adjustment	34.7656	0.9788	0.0432

In the second convolution layer, a 3*3 kernel with the step size of 1 is used, and the filters are reduced to 64. In the third layer, a convolution layer with the size of 3*3 and step size of 2 is used to reduce the size of the image in order to decrease computational burden. A total of 8 residual blocks are set in layers 4th to 19th layers. Each residual block sets a short connection between two convolution layers. The convolution layers in the residual block are all of kernel size of 3*3, step size of 1, and filter size of 64. The 20th layer is a deconvolution layer with kernel size of 3*3 and step size of 2. The 21st and 22nd layers use convolution layer images with a kernel size of 3*3 and filter of 1. The established model uses ReLU as the activation function except for the last convolution layer, which does not use activation function.

Firstly, from the infrared image dataset LTIR v1.0 [29], 1825 images are randomly selected and cropped into 50*50 image patches, and the cropped image blocks are randomly rotated and then the image blocks were corrupted by using a non-uniformity with mean 0 and standard deviation from 0 to 0.15 according to (1). Finally more than 480,000 image patches are obtained to form the training set. The 269 consecutive infrared images were used as testing set 1. The simulation of the infrared non-uniformity images were achieved by adding the infrared non-uniformity with mean value of 0 and standard deviation of 0.15 for the images of test set 1 according to (1).

4.2 Training

The most widely used loss function in image processing are L1 and L2. Compared with L1, L2 has a stable solution and higher computational efficiency, therefore, the average mean square error is used as the loss function, its expression is the average square error between the estimated residual image and expected input noise image, as shown in (4).

$$L = \frac{1}{2n} \sum_{i=1}^n \|F(y_i) - (y_i - x_i)\|_F^2 \quad (4)$$

where n denotes the batch size in the network, y_i represents the input images including noise, x_i represents clean input images, and $F(y_i)$ is the residual mapping of the image y_i .

Training is carried out by using the Adam optimizer with a batch of 128 sub-images to optimize the loss function. The initial learning rate of the model is set to 0.001, and it drops to tenth of the previous learning rate every 40 epochs.

All experiments are carried out in the Python 3.6.8 and Tensorflow 2.2.0 environment with 50 epochs, and run on a PC with Intel(R) Core(TM) i7-8750H CPU 2.20 GHz and Nvidia GTX 1060 GPU. The performance comparison curves with or without short connections are shown in Fig. 3. Comparison of average results for 269 frames with or without long and short connections and with or without size adjustment results are shown in Table 2.

The model with short connections and size adjustment achieves the highest values for peak signal-to-noise ratio (PSNR) and structural similarity index measure (SSIM) at the vast majority of frames, as shown in Fig. 3(a) and Fig. 3(b). In Fig. 3(c), the model without size adjustment takes significantly more time, while the other two models take about the same time.

In Table II, the proposed model achieves the highest values of 37.5128 dB and 0.9808 for both PSNR and SSIM, compared with the model without size adjustment, the PSNR of the proposed

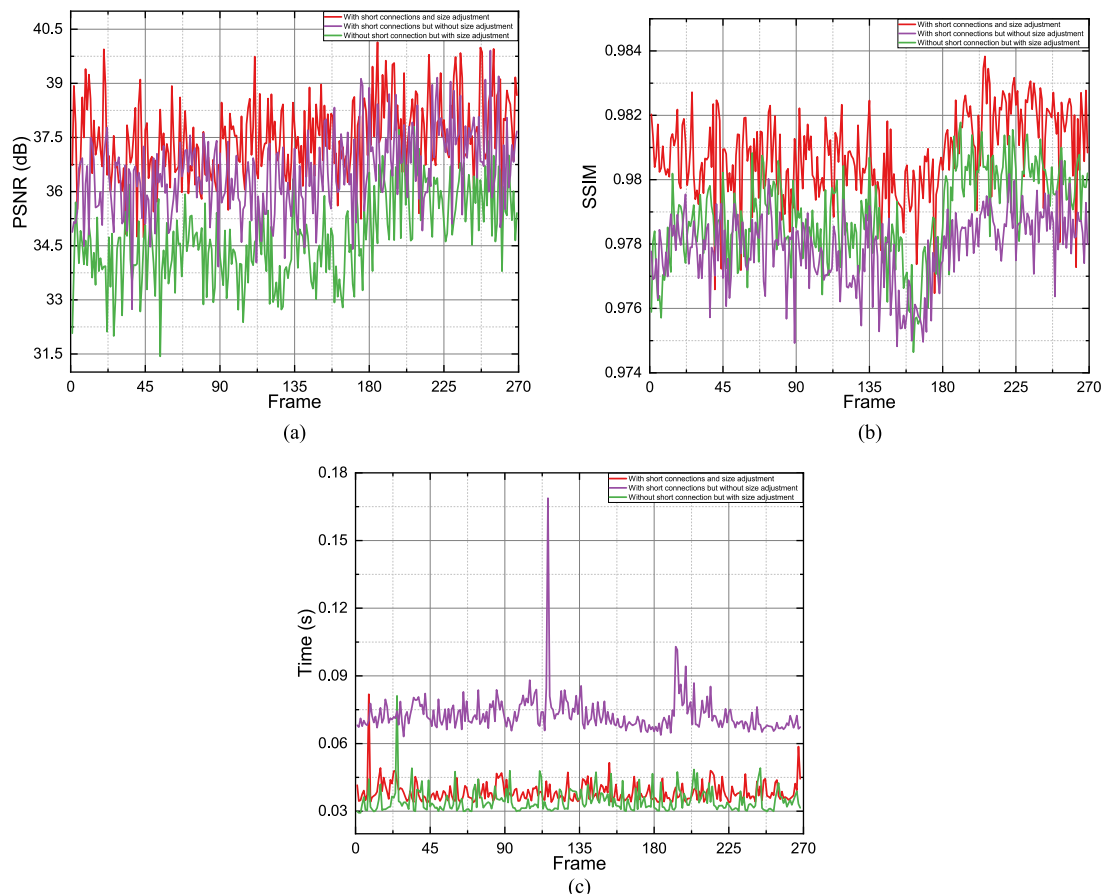


Fig. 3. Comparison with or without long and short connections and with or without size adjustment results. (a) PSNR (b) SSIM (c) Time.

model improved by 0.99 dB, the SSIM improved by 0.003, and the time is reduced by 0.0282 seconds. The PSNR of the proposed method is about 2.75 dB higher than that of the method without short connections, and the SSIM is about 0.002 higher, while the processing time of a single-frame image with short connections is only about 0.0013 seconds slower.

4.3 Qualitative Evaluation

Experiments are validated by using a simulation video dataset with a resolution of 320*240 and a total of 269 frames. Frame 110 and frame 225 are randomly selected for comparison. The 110th frame effect is shown in Fig. 4. GF in Fig. 4(c) has a great quality residual noise in the test results, and it is almost impossible to observe the background information, accompanied by the distortion of the characters in the image. Fig. 4(d) is the test results of SNRCNN, in which the residual noise is still visible, the human arm cannot be seen in the mirror behind the person and the edges of the wall behind the person are blurred. The visual effect of DnCNN in Fig. 4(e) has been greatly improved, but there is still some residual noise. In Fig. 4(f), the residual noise of DLS-NUC is further reduced, but distortion occurs at the edges of the human torso, arms and head. Fig. 4(g) shows that LSC-CNN can scarcely observe the presence of residual noise, the arms of the person in the mirror are clearly visible, and the edge information of the person in the image is effectively preserved.

The results of 225th frame are shown in Fig. 5. In Fig. 5(c), there are more severe distortions in the face and significant residual noises in the image, and the background can hardly be observed

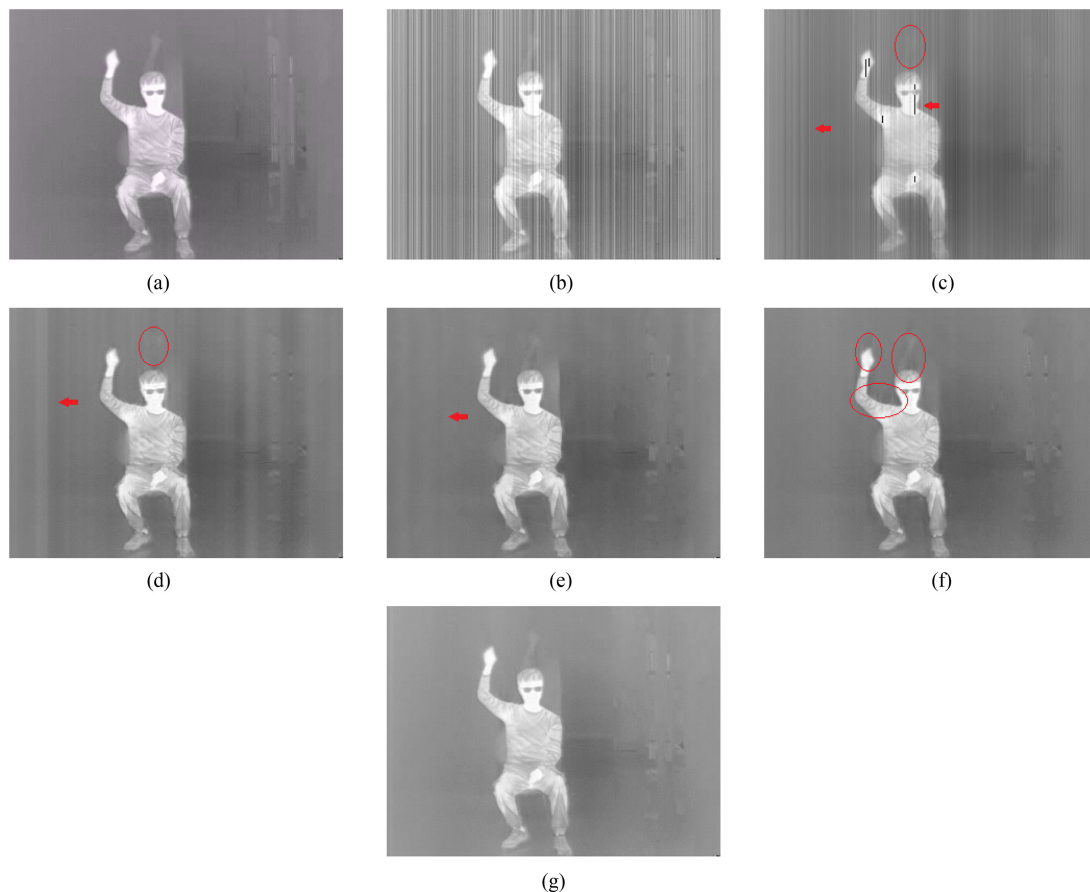


Fig. 4. 110th frame of the simulated infrared image test results. (a) Original image. (b) Noisy image. (c) GF. (d) SNRCNN. (e) DnCNN. (f) DLS-NUC. (g) LSC-CNN.

except the chair after GF correction. The image corrected by SNRCNN is Fig. 5(d), which contains more residual noises, but some details in the background have been retained. The result of DnCNN is shown in Fig. 5(e), there are some residual noises in the head and chair. In Fig. 5(f), DLS-NUC effectively removes noise, but the corrected image shows that the door frame behind the chair is indistinguishable from the wall. In Fig. 5(g), not only the residual noise can scarcely be observed by LSC-CNN, but also the background information in the original image is preserved well.

The proposed LSC-CNN method is evaluated by 192×130 real infrared images [30], and the comparison results are shown in Fig. 6. FPN is removed by GF as shown in Fig. 6(b), but the image becomes blurred, some detailed information in the original image are lost, and the branches in the lower left corner of the picture cannot be accurately identified. In the Fig. 6(c), SNRCNN effectively corrects the non-uniformity in the original image, but loses a great deal of detail information of the original image, for instance, the edges of walls and windows become blurred. Fig. 6(d) shows that the image processed by DnCNN is not smooth enough, and the image has certain sense of graininess. After DLS-NUC processing, as shown in Fig. 6(e), the contrast of the whole image is reduced, resulting in the boundaries blurring between the wall, window and sash. Fig. 6(f) shows the corrected image of LSC-CNN. Compared with other methods, LSC-CNN effectively corrects the non-uniformity of the original image while retaining the image edge information with less graininess, and the window sash in the corrected image can also be clearly observed.

The raw infrared image [30] of 320×220 is used to test these methods, and the comparison results are shown in Fig. 7. In Fig. 7(b), the image processed by GF is particularly blurry and

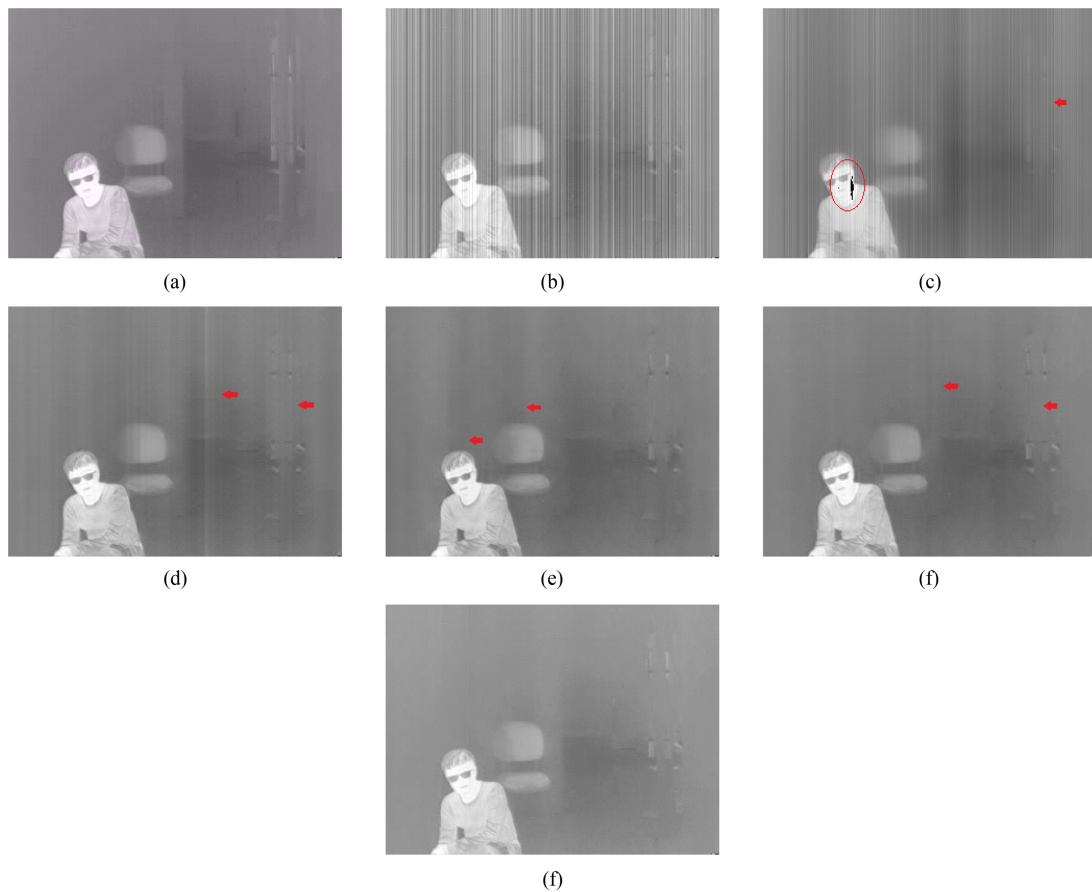


Fig. 5. 225th frame of the simulated infrared image test results. (a)Original image. (b) Noisy image. (c) GF. (d) SNRCNN. (e) DnCNN. (f) DLS-NUC. (g) LSC-CNN.

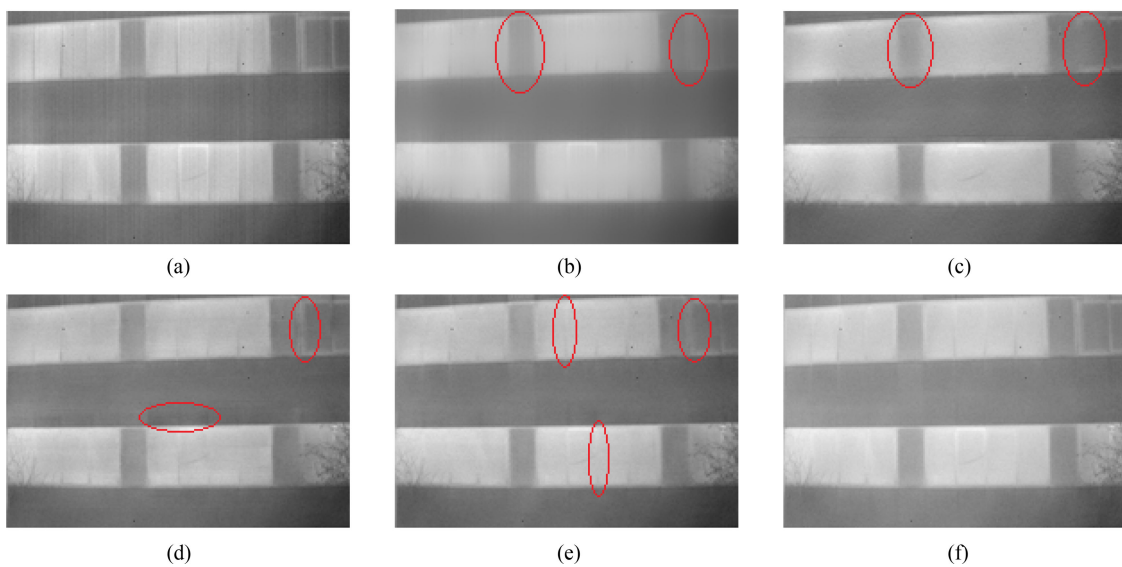


Fig. 6. Real infrared image 1 test results. (a)Original image. (b) Noisy image. (c) GF. (d) SNRCNN. (e) DnCNN. (f) DLS-NUC. (g) LSC-CNN.

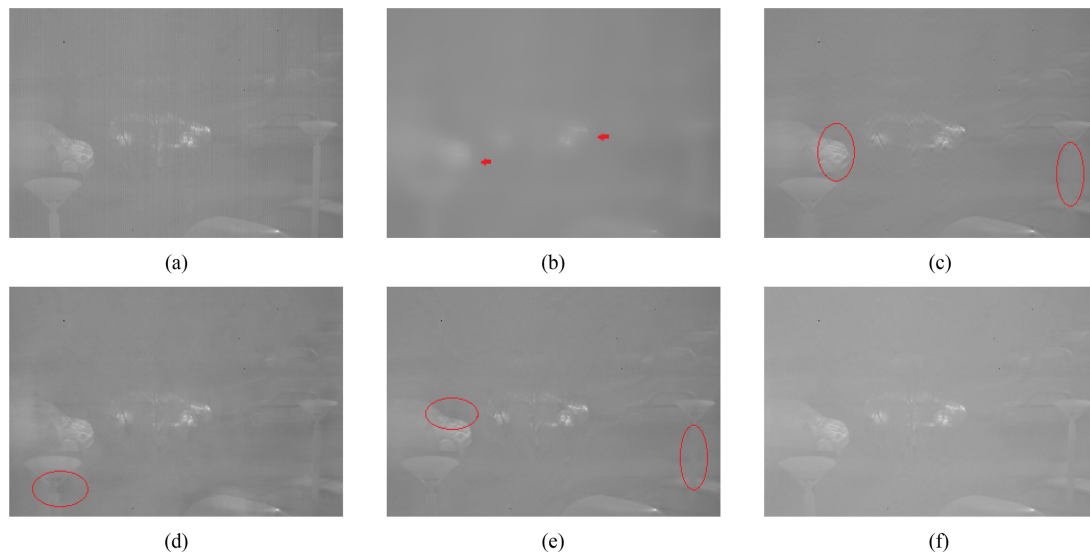


Fig. 7. Real infrared image 2 test results. (a)Original image. (b) Noisy image. (c) GF. (d) SNRCNN. (e) DnCNN. (f) DLS-NUC. (g) LSC-CNN.

cannot accurately distinguish the information in the image. In Fig. 7(c), the image corrected by SNRCNN has obvious distortion, which has a certain impact on the visual effect. In Fig. 7(d), the result of DnCNN shows that there are a small amount of residual noises and significant granularity. In Fig. 7(e), the image processed by DLS-NUC is smoother than by DnCNN, however, the issue of low contrast exists, as a result, it is difficult to distinguish the edges of the overlap between the lamp post in the lower right corner and the ground in the background. In Fig. 7(f), as compared to these methods, LSC-CNN has achieved the best visual results in image clarity and detail preservation.

According to the simulated infrared video and real infrared non-uniformity images, it can be found that GF will cause images distortion in the case of large non-uniformity and will cause the images blurred in the case of low contrast. The SNRCNN method has significant noise residual in large non-uniformity, and the method causes large loss of edge information and detail information of the images. The DnCNN method still has obvious non-uniformity in the corrected image, and the corrected images have significant graininess. The DLS-NUC method causes a certain distortion of the target edges in images with large non-uniformity, while detail information loss appears in images with small non-uniformity. The proposed LSC-CNN method can hardly find the residual noise in the corrected images, and it can protect the detail information and edge information of the images effectively.

The advantages of the proposed method can be seen from the above comparative tests. Compared with the shallower SNRCNN, LSC-CNN can learn the images detail information more sufficiently. Compared with the non-neural network method GF, LSC-CNN has significantly improved correction effect and detail preservation. With the increase of the network depth, the number of parameters will increase significantly and lead to the increase of the model computation time. Therefore, LSC-CNN reduces the computation by decreasing the size of the images in the model and restoring the images to their original size by the transpose convolution. In order to solve the problem of image information loss caused by transposed convolution, the input layer information will be used to compensate the image after transpose convolution. Considering that infrared images have lower image resolution and contrast compared to visible images, and different from DnCNN and DLS-NUC, LSC-CNN enhances the contrast of the image by using a per-pixel multiplication of the images before and after compensation, which effectively improved the contrast of images.

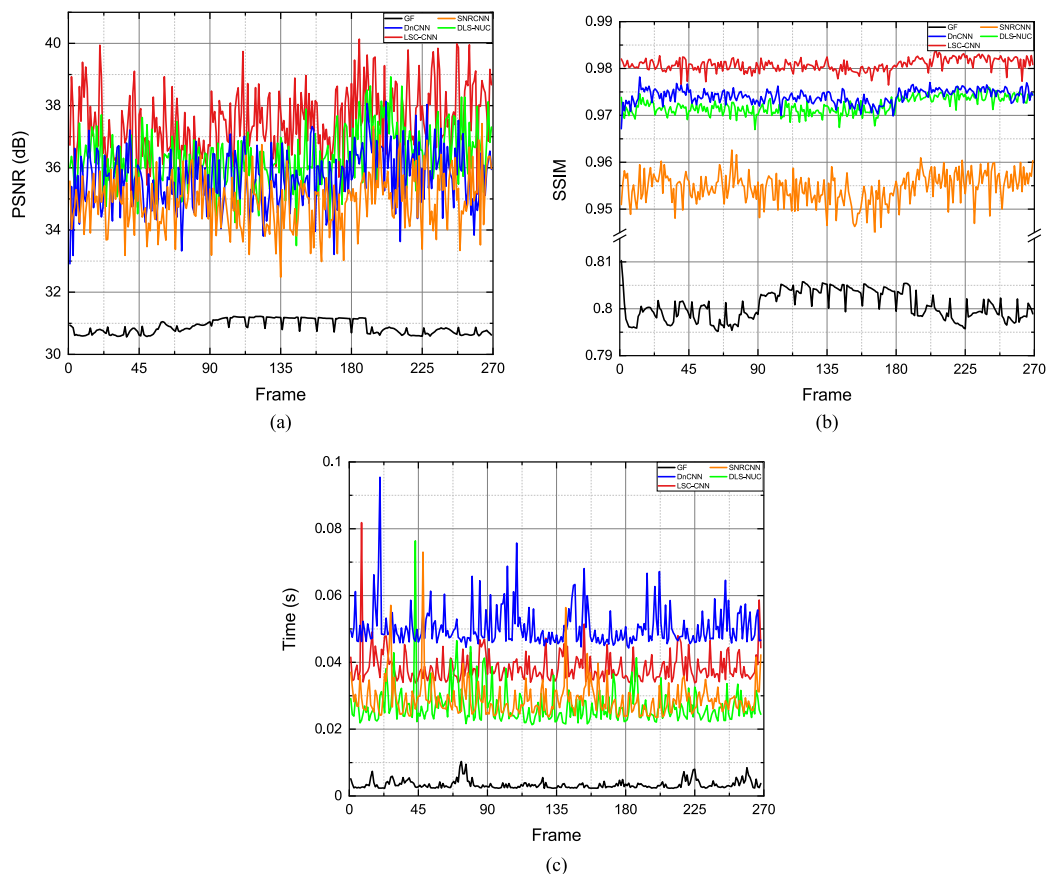


Fig. 8. PSNR, SSIM and Time of GF, SNRCNN, DnCNN, DLS-NUC and LSC-CNN tested in all 269 frames. (a) PSNR (b) SSIM (c) Time.

4.4 Quantitative Evaluation

For quantitative validation of the performance, the images are evaluated by using PSNR [31], [32], as shown in (5) and (6).

$$PSNR = 10 \log_{10} \left(\frac{L^2}{MSE} \right) \quad (5)$$

$$MSE(x, y) = \frac{1}{N} \sum_{i=1}^N (x_i - y_i)^2 \quad (6)$$

where MSE is the mean square error of the image, x and y are the images to be calculated, N is the number of pixels, x_i and y_i represent the i -th pixel in x and y , and L is the maximum pixel value of the image (L is 255 for unit8 data or 1 for float-point data).

PSNR values of the corrected 269 frames of the image are shown in Fig. 8(a), where the highest PSNR value tested by GF does not exceed 32 dB. Some PSNR values the images processed by SNRCNN are below 34 dB. The overall PSNR values processed by DnCNN are below 36 dB, which is slightly higher than SNRCNN. PSNR values processed by DLS-NUC are mostly above 36 dB, and are higher than by LSC-CNN in a few individual frames, but the LSC-CNN achieves the highest values in the vast majority of the images, and the highest values are above 40 dB.

The larger value of PSNR indicates less distortion of a image, but the evaluation criteria of PSNR differs from the human visual system (HVS), which probably causes images with a higher PSNR to look worse than those with a lower PSNR, so the corrected results are also evaluated by SSIM [33]

TABLE 3
Average Results After 269 Frames of Video Test

Models	GF	SNRCNN	DnCNN	DLS-NUC	LSC-CNN
AVG PSNR	30.8877	34.9437	35.6844	36.3673	37.5128
AVG SSIM	0.8006	0.9546	0.9741	0.9721	0.9808
AVG Time	0.0034	0.0373	0.0563	0.0338	0.0445

TABLE 4
Real Infrared Image 1 Test Results

Models	GF	SNRCNN	DnCNN	DLS-NUC	LSC-CNN
PSNR	30.4678	34.4688	30.8249	34.0998	35.5526
SSIM	0.9024	0.9282	0.9322	0.9424	0.9624
Time	0.0019	0.0221	0.0286	0.0220	0.0234

TABLE 5
Real Infrared Image 2 Test Results

Models	GF	SNRCNN	DnCNN	DLS-NUC	LSC-CNN
PSNR	37.4017	38.7784	35.2226	39.2569	39.8212
SSIM	0.8897	0.9211	0.9157	0.9147	0.9207
Time	0.0025	0.0236	0.0419	0.0220	0.0321

which is more consistent with HVS, as shown in (7).

$$SSIM(x, y) = \frac{(2\mu_x\mu_y + C_1)(2\sigma_{xy} + C_2)}{(\mu_x^2 + \mu_y^2 + C_1)(\sigma_x^2 + \sigma_y^2 + C_2)} \quad (7)$$

where x and y denote the two images in which the calculations are performed, μ_x and μ_y represent the mean of x and y respectively, σ_x^2 and σ_y^2 are the variances of x and y respectively, σ_{xy} is the covariance of x and y , C_1 and C_2 are constants that avoid division by zero.

The parameters for calculating SSIM are the same as those given in [33], and the results are shown in Fig. 8(b). The evaluation values of GF are still the lowest and have a large gap with other methods, whose highest value is less than 0.81. The evaluation values of SNRCNN are mostly below 0.96. The evaluation values of DnCNN and DLS-NUC are close and both above 0.97. LSC-CNN achieves the highest value in all the images tested and is approximately 0.98, which is closer to the original image and more in conformity with HVS than other methods.

Fig. 8(c) records the time taken for each image denoising in the test. Although the speed of GF has great advantages, its correction effect is unsatisfactory, so it is not applicable to the non-uniformity correction of infrared images. SNRCNN and DLS-NUC take almost the same time. LSC-CNN is slightly slower than SNRCNN and DLS-NUC, but faster than DnCNN.

The test results of 269 frames are statistically calculated to compare the average values, as shown in Table 3. The average PSNR of LSC-CNN is more than 1 dB higher than other existing methods and the SSIM mean value exceeds 0.98. Although LSC-CNN is somewhat slower than SNRCNN and DLS-NUC, by taking the image quality improvement into consideration, LSC-CNN is still very competitive.

The validation results carried out on real infrared images are shown in Table 4 and Table 5. For the real infrared images 1 (Fig. 6(a)), LSC-CNN achieves the highest values in PSNR and SSIM which greatly exceed other existing models, and significantly reduce the processing time in the small size images. In the test of real infrared image 2 (Fig. 7(a)), although the SSIM value of LSC-CNN is 0.0004 less than that of SNRCNN, in view of the distortion in the image of SNRCNN, LSC-CNN is still preferable to other existing correction methods. In the meanwhile, the processing time of LSC-CNN in processing real infrared images is obviously shorter than the processing time of simulated images.

5. Conclusion

In this paper, an improved non-uniformity correction method of infrared images based on convolution neural network using long-short connections, LSC-CNN, is proposed, which uses a residual network and introduces short connect into the infrared image non-uniformity correction. LSC-CNN is a scene-based non-uniformity correction method, which can solve the problem that the calibration-based method is unable to work continuously for a long time. Compared with existing visible image denoising methods and non-uniformity correction methods, LSC-CNN provides more accurate and comprehensive denoising of infrared images by enhancing the corrected images, while better preserving the edge and detail information of the images. The video tests have verified that LSC-CNN does not produce artifact, and the real infrared images have verified that LSC-CNN has excellent correction effect. LSC-CNN can be applied to more image correction fields, and can be further optimized and lightweight in the future to improve the computing speed.

Acknowledgment

The authors would also like to thank the anonymous reviewers for their valuable suggestions.

References

- [1] E. Wang, P. Jiang, X. Hou, Y. Zhu, and L. Peng, "Infrared stripe correction algorithm based on wavelet analysis and gradient equalization," *Appl. Sci.*, vol. 9, no. 10, 2019, Art. no. 1993.
- [2] S. Chang and Z. Li, "Calibration algorithm for cooled mid-infrared systems considering the influences of ambient temperature and integration time," *Appl. Opt.*, vol. 58, no. 29, 2019, Art. no. 8118.
- [3] Y. Chang, L. Yan, L. Liu, H. Fang, and S. Zhong, "Infrared aerothermal nonuniform correction via deep multiscale residual network," *IEEE Geosci. Remote Sens. Lett.*, vol. 16, no. 7, pp. 1120–1124, Jul. 2019.
- [4] R. Sheng-Hui, Z. Hui-Xin, Q. Han-Lin, L. Rui, and Q. Kun, "Guided filter and adaptive learning rate based non-uniformity correction algorithm for infrared focal plane array," *Infrared Phys. Technol.*, vol. 76, pp. 691–697, 2016.
- [5] Q. Wu, W. Ren, and X. Cao, "Learning interleaved cascade of shrinkage fields for joint image dehazing and denoising," *IEEE Trans. Image Process.*, vol. 29, pp. 1788–1801, 2020.
- [6] Z. Fan, D. Bi, S. Gao, L. He, and W. Ding, "Adaptive enhancement for infrared image using shearlet frame," *J. Opt.*, vol. 18, no. 8, Jul. 2016, Art. no. 085706.
- [7] X. Bai, "Morphological infrared image enhancement based on multi-scale sequential toggle operator using opening and closing as primitives," *Infrared Phys. Technol.*, vol. 68, pp. 143–151, 2015.
- [8] K. He, J. Sun, and X. Tang, "Guided image filtering," in *Proc. Eur. Conf. Comput. Vis.*, 2010, pp. 1–14.
- [9] K. Dabov, A. Foi, V. Katkovnik, and K. Egiazarian, "Image denoising by sparse 3-D transform-domain collaborative filtering," *IEEE Trans. Image Process.*, vol. 16, no. 8, pp. 2080–2095, Aug. 2007.
- [10] K. Zhang, W. Zuo, Y. Chen, D. Meng, and L. Zhang, "Beyond a Gaussian denoiser: Residual learning of deep CNN for image denoising," *IEEE Trans. Image Process.*, vol. 26, no. 7, pp. 3142–3155, Jul. 2017.
- [11] S. Chang and Z. Li, "Single-reference-based solution for two-point nonuniformity correction of infrared focal plane arrays," *Infrared Phys. Technol.*, vol. 101, pp. 96–104, 2019.
- [12] N. Chen, J. Zhang, S. Zhong, W. Mao, and L. Yao, "Two-dimensional calibration for fixed-pattern noise reduction of thermal images," in *Proc. IEEE Int. Symp. Circuits Syst.*, 2019, pp. 1–5.
- [13] F. Marcotte, P. Tremblay, and V. Farley, "Infrared camera NUC and calibration: Comparison of advanced methods," *Proc. Spie*, vol. 8706, pp. 17–26, 2013.
- [14] B. Sofu, D. U. Sakarya, and O. Akn, "Comparison of non-uniformity correction methods in midwave infrared focal plane arrays of high speed platforms," in *Proc. Appl. Digit. Image Process. XLI*, 2018, pp. 20–31.
- [15] B. M. Ratliff, M. M. Hayat, and J. S. Tyo, "Radiometrically accurate scene-based nonuniformity correction for array sensors," *J. Opt. Soc. Amer. A*, vol. 20, no. 10, pp. 1890–1899, 2003.
- [16] A. Ferrero, J. Campos, and A. Pons, "Correction of photoresponse nonuniformity for matrix detectors based on prior compensation for their nonlinear behavior," *Appl. Opt.*, vol. 45, no. 11, pp. 2422–2427, 2006.
- [17] S. N. Torres and M. M. Hayat, "Kalman filtering for adaptive nonuniformity correction in infrared focal-plane arrays," *J. Opt. Soc. Amer. A Opt. Image Sci. Vis.*, vol. 20, no. 3, pp. 470–80, 2003.
- [18] J. Jia, Y. Wang, X. Cheng, L. Yuan, and J. Wang, "Destriping algorithms based on statistics and spatial filtering for visible-to-thermal infrared pushbroom hyperspectral imagery," *IEEE Trans. Geosci. Remote Sens.*, vol. 57, no. 6, pp. 4077–4091, Jun. 2019.
- [19] W. Hua *et al.*, "Stripe nonuniformity correction for infrared imaging system based on single image optimization," *Infrared Phys. Technol.*, vol. 91, pp. 250–262, 2018.
- [20] Y. Yuan, Q. Song, X. Guo, and Y. Wang, "A new temporal high-pass adaptive filter nonuniformity correction based on rolling guidance filter," in *Proc. MIPPR 2019: Multispectral Image Acquisition, Process., Anal.*, vol. 11428, 2020, Art. no. 114280L.
- [21] J. Guan, R. Lai, A. Xiong, Z. Liu, and L. Gu, "Fixed pattern noise reduction for infrared images based on cascade residual attention CNN," *Neurocomputing*, vol. 377, no. 15, pp. 301–313, Feb. 2020.

- [22] R. Lai, G. Yue, and G. Zhang, "Total variation based neural network regression for nonuniformity correction of infrared images," *Symmetry*, vol. 10, no. 5, 2018.
- [23] R. Lai, J. Guan, Y. Yang, and A. Xiong, "Spatiotemporal adaptive nonuniformity correction based on BTV regularization," *IEEE Access*, vol. 7, pp. 753–762, 2019.
- [24] X. Kuang, X. Sui, Q. Chen, and G. Gu, "Single infrared image stripe noise removal using deep convolutional networks," *IEEE Photon. J.*, vol. 9, no. 4, Aug. 2017, Art. no. 7800615.
- [25] Y. Li, W. Jin, J. Zhu, X. Zhang, and S. Li, "An adaptive deghosting method in neural network-based infrared detectors nonuniformity correction," *Sensors*, vol. 18, no. 1, 2018, Art. no. 211.
- [26] Q. Li, B. Yang, X. Wang, L. Liu, C. Liu, J. Su, "Neural network non-uniformity correction for eliminating low frequency noise," in *Proc. 5th Conf. Frontiers Opt. Imag. Technol. Appl.*, 2018, Art. no. 1083207.
- [27] Z. He *et al.*, "Single-image-based nonuniformity correction of uncooled long-wave infrared detectors: A deep-learning approach," *Appl. Opt.*, vol. 57, no. 18, pp. D155–D164, 2018.
- [28] J. Guan, R. Lai, and A. Xiong, "Wavelet deep neural network for stripe noise removal," *IEEE Access*, vol. 7, pp. 44544–44554, 2019.
- [29] A. Berg, J. Ahlberg, and M. Felsberg, "A thermal object tracking benchmark," in *Proc. IEEE Int. Conf. Adv. Video Signal Based Surveill.*, 2015, pp. 1–6.
- [30] Y. Tendero, S. Landeau, and J. Gilles, "Non-uniformity correction of infrared images by midway equalization," *Image Process. Line*, vol. 2, pp. 134–146, 2012.
- [31] Q. L. Zhou Wang, "Video quality assessment using a statistical model of human visual speed perception," *J. Opt. Soc. Amer. A Opt. Image Sci. Vis.*, vol. 24, no. 12, pp. 61–69, 2007.
- [32] W. Zhou and A. C. Bovik, "Mean squared error: Love it or leave it? A new look at signal fidelity measures," *IEEE Signal Process. Mag.*, vol. 26, no. 1, pp. 98–117, Jan. 2009.
- [33] Wang *et al.*, "Image quality assessment: From error visibility to structural similarity," *IEEE Trans. Image Process.*, vol. 13, no. 4, pp. 600–612, Apr. 2004.